Using colloidal lithography to fabricate and optimize sub-wavelength pyramidal and honeycomb structures in solar cells

H. L. Chen[1*], S. Y. Chuang[1], C. H. Lin[2], and Y. H. Lin[1]

[1]*Department of Materials Science and Engineering, National Taiwan University, Taipei, Taiwan*
[2]*National Nano Device Laboratory, 1001-1 Ta Hsueh Road Hsinchu, Taiwan*
hsuenlichen@ntu.edu.tw

Abstract: The external quantum efficiency of solar cells can be improved by using texturing pyramid- and honeycomb-like structures with minimum reflection. In this study, we investigated the reflection properties of texturing structures through rigorous coupled-wave analysis and the three-dimensional finite-difference time domains (FDTD) method to analyze close-packed texturing structures. We also demonstrate a simple method—combining sub-wavelength-scale monolayer and bilayer polystyrene spheres with a one-step reactive ion etching process—to fabricate optimized pyramid- and honeycomb-shaped antireflection structures, respectively. Thus, sub-wavelength pyramidal and honeycomb-like structures displaying low reflectance were obtained readily without the need for any lithography equipment.

©2007 Optical Society of America

OCIS codes: (310.1210) Antireflection; (230.4000) Microstructure fabrication; (040.6040) Silicon.

References and links

1. I. M. Dharmadasa, "Third generation multi-layer tandem solar cells for achieving high conversion efficiencies," Sol. Energ. Mat. Sol. C. **85**, 293-300 (2005).
2. M. A. Green, K. Emery, D. L. King, S. Igari, and W. Warta, "Solar cell efficiency tables, " Prog. Photovoltaics **11,** 39-45 (2003).
3. S. Siebentritt, "Wide gap chalcopyrites: material properties and solar cells," Thin Solid Films. **403-404,** 1-8 (2002).
4. E. D. Palik, in *Handbook of Optical Constants of Solids*, Academic Press (1998).
5. H. A. Macleod, in *Thin-Film Optical Filters*, 2nd Ed., Adam Hilger Ltd. (1986).
6. B. Kumar, T. B. Pandian, E. Sreekiran, and S. Narayanan, "Benefit of dual layer silicon nitride antireflection coating," in Proceedings of IEEE Conference on Photovoltaic Specialists, 1205-1208 (2005).
7. D. H. Macdonald, A. Cuevas, C. Samundsett, D. Ruby, S. Winderbaum and A. Leo, "Texturing industrial multicrystalline silicon solar cells," Sol. Energ. Mat. Sol. C. **80**, 227-237 (2004).
8. J. D. Hylton, A. R. Burger, and W. C. Sinke, "Alkaline etching for reflectance reduction in multicrystalline silicon solar cells," J. Electrochem. Soc. **151**, 408-427 (2004).
9. R. Bilyalov, L. Stalmans, and J. Poortmans, "Comparative analysis of chemically and electrochemically formed porous Si antireflection coating for solar cells," J. Electrochem. Soc. **150**, 216-222 (2003).
10. K. Kintaka, J. Nishii, A. Mizutani, H. Kikuta, and H. Nakano, "Antireflection microstructures fabricated upon fluorine-doped SiO_2," Opt. Lett. **26,** 1642-11644 (2001).
11. Z. Yu, H. Gao, W. Wu, H. Ge, and S. Y. Chou, "Fabrication of large area subwavelength antireflection structures on Si using trilayer resist nanoimprint lithography and liftoff," J. Vac. Sci. Technol. B. **21**, 2874-2877 (2003).
12. S. H. Zaidi, D. S. Ruby, and J. M. Gee, "Characterization of random reactive ion etched-textured silicon solar cells," Electron Devices, IEEE Transactions **48,** 1200-1206 (2001).
13. J. Zhao, A. Wang, and M. A. Green, "19.8% efficient 'honeycomb' textured muticrystalline and 24.4% monocrstalline silicon solar cells," Appl. Phys. Lett. **78,** 1991-1993 (1998).
14. L. Li, "New formulation of the Fourier modal method for crossed surface-relief gratings," J. Opt. Soc. Am. A. **14,** 2758-2767 (1997).

15. C. Brückner, B. Pradarutti, O. Stenzel, R. Steinkopf, S. Riehemann, G. Notni, and A. Tünnermann, "Broadband antireflective surface-relief structure for THz optics," Opt. Express **15,** 779-789 (2007), http://www.opticsinfobase.org/abstract.cfm?URI=oe-15-3-779.
16. C. H. Lin, H. L. Chen, W. C. Chao, C. I. Hsieh and W. H. Chang, "Optical characterization of two-dimensional photonic crystals based on spectroscopic ellipsometry with rigorous coupled-wave analysis," Microelectron. Eng. **83,** 1798–1804 (2006).
17. A. K. Wong, "*Resolution enhancement techniques*," The International Society for Optical Engineering (SPIE) (2001).
18. S. M. Yang, S. G. Jang, D. G. Choi, S. Kim, and H. K. Yu, "Nanomachining by colloidal lithography," Small **2,** 458-475 (2006).
19. J. H. Moon, S. G. Jang, J. M. Lim, and S. M. Yang, "Multiscale nanopatterns templated from two-dimensional assemblies of photoresist particles," Adv. Mater. **17,** 2559-2562 (2005).
20. A. Kosiorek, W. Kandulski, H. Glaczynska, and M. Giersig, "Fabrication of nanoscale rings, dots, and rods by combining shadow nanosphere lithography and annealed polystyrene nanosphere masks," Small **1,** 439-444, (2005).
21. D. L. J. Vossen, D. Fific, J. Penninkhof, T. Dillen, A. Polman, and A. Blaaderen, "Combing optical tweezers/ion beam technique to tune colloidal masks for nanolithography," Nano Lett. **5,** 1175-1179 (2005).
22. Y. Zhao, J. Wang, and G. Mao, "Colloidal subwavelength nanostructures for antireflection optical coatings," Opt. Lett. **30,** 1885-1887 (2005).
23. H. Xiao, in *Introduction to Semiconductor Manufacturing Technology,* Prentice Hall Inc. (2001).

1. Introduction

The development of highly efficient solar cells is one solution to the problems of energy depletion and environmental destruction. Many kinds of solar cells have been investigated in terms of their efficiency, cost, duration, and reliability [1, 2]; among them, the silicon-based solar cells, which have been known for quite a while, appear to be strong candidates for future development because of their mature fabrication techniques and relatively low cost. Recently, other semiconductor-based solar cells utilizing gallium arsenide, indium phosphide, and germanium have been investigated intensively to exploit their high quantum efficiencies and ready construction of intermediate band structures [2, 3]. All of these semiconductor materials have high refractive indices in the regime from the visible to the near-infrared (NIR), resulting in high Fresnel reflection at their air–semiconductor interfaces [4, 5]. Therefore, a key issue toward increasing the external quantum efficiency (EQE) of semiconductor-based solar cells is determining methods to reduce interfacial reflection in the solar cell working-wavelength regime.

Much research has been undertaken toward the goal of reducing the reflectance of silicon-based solar cells. A common method is the application of a single-layer antireflective coating, such as a single-layer silicon nitride or silicon oxynitride film. This technique cannot be employed, however, for cells that operate over a broad range of wavelengths; in addition, the thicknesses and optical constants of multilayer optical thin films must be controlled well for broadband antireflection coatings [5, 6]. Conventionally, wet etching methods, utilizing alkaline solutions such as KOH or tetramethylammonium hydroxide (TMAH), are employed to fabricate V-groove antireflective structures on single-crystal silicon surfaces. By taking advantage of the different etching rates between the <100> and <111> surfaces of silicon crystals, the V-groove profile and surface roughness can be controlled by varying the concentration of the alkaline solution [7]. For multicrystalline substrates, this method is less practicable because of the presence of various crystallographic grain orientations [8]. Reactive ion etching (RIE) utilizing chlorine or SF_6/O_2 is an alternative method for the formation of textured structures on multi- and single-crystalline silicon substrates [9, 10]. Nevertheless, the surface profile of a solar cell is strongly dependent on the conditions of the RIE process. Although imprint lithography had been used to fabricate sub-wavelength antireflective structures [11], the need for complicated triple-layer resist processes would decrease the throughput and reliability of the approach.

Previous research indicates that the optimum antireflection structures of solar cells are close-packed pyramidal and honeycomb-like arrays not in sub-wavelength scale for the difficulty of fabrication [12, 13]. Recently, surface-relief gratings have been used as broadband antireflective structures in the THz regime [14]. In this study, we used rigorous coupled-wave analysis (RCWA) and finite-difference time domains (FDTD) methods to analyze the reflection properties of two-dimensional microstructures [15, 16]. We found that the reflectance increased dramatically as consideration of the diffraction order of the textured structures. Therefore, to obtain high-performance solar cells it is important to pattern sub-wavelength textures and close-packed structures to eliminate all diffraction-order light. Generally, sub-wavelength structures should be patterned using a deep-ultraviolet (DUV) exposure tool in conjunction with resolution-enhancement techniques [17]. Furthermore wet or dry etching processes typically occur randomly without the formation of sub-wavelength close-packed structures.

Colloidal lithography is a low-cost and relatively high-throughput technique for patterning nanostructures. The advantage of colloidal lithography in nanofabrication is that large-area self-assembly of colloids having well-ordered structures can be performed without the need for expensive equipment [18, 19]. Recently, nanostructures such as rings, dots, and rods have been fabricated using colloidal lithography [20, 21]. Exploiting the index-matching concept, monolayer nanoparticles also have been used for the antireflective layer on glass substrates that lack optimally textured structures [22]. In this paper, we demonstrate a simple method—one that combines close-packed monolayer and bilayer nanospheres with an optimal one-step reactive ion etching process—for fabricating and optimizing the performance of pyramidal and honeycomb-like antireflection structures in sub-wavelength scales. We believe that colloidal lithography has great potential for use in the preparation of high-performance textured structures in large-area solar cells at low cost and with high reproducibility.

2. Simulation and Experiment Setup

In this study, we used a rigorous coupled-wave analysis to simulate reflection and transmission properties in two-dimensional microstructures. This approach has been used widely to analyze the optical diffraction of the periodic structures displayed in Fig. 1(a), solving Maxwell's equations in a periodic medium after applying the field and permittivity.

Figure 1(b) indicates that the pyramidal structure with period Λ and height h was divided vertically a gradient size for the RCWA simulation. Furthermore, the three-dimensional FDTD method was used to analyze the optical behavior of reflective light on the textured structures within the near-field regime. To fabricate the optimal antireflection structure, textured structures with different periods and heights were simulated. The experimental parameters were established accordingly. In the experimental procedures, silicon substrates were coated with close-packed polystyrene spheres using a dip coater. The patterned close-packed polystyrene spheres were then transferred to the silicon substrate using a reactive ion etcher (Anelva, ECR-6001) and Cl_2, SF_6, and O_2 as reactive gases. Cross-sectional profiles were observed using a scanning electron microscope (JEOL, JSM-6500F); the optical properties were measured using an optical spectrometer (Hitachi, U-4100).
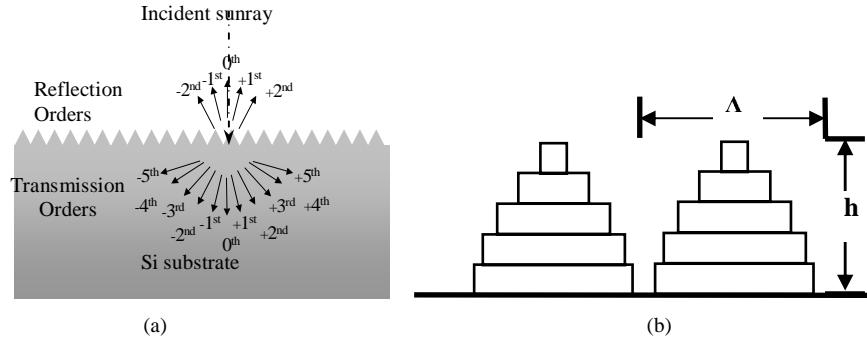
Fig. 1. Schematic illustrations of (a) the reflection and transmission diffraction orders for incident rays of light upon interaction with a pyramidal structure and (b) the pyramidal structures utilized for rigorous coupled-wave simulation.

3. Results and Discussion

Figure 2(a) indicates that the reflectance from 300 to 900 nm was less than 3% when considering only the zeroth-order reflection of the pyramidal structure having a period of 800 nm and a height of 450 nm. When considering all diffraction orders, the reflectance increased dramatically at wavelengths less than 800 nm. Similarly, Fig. 2(b) indicates that the reflectance was less than 3% at wavelengths from 350 to 900 nm when considering all diffraction orders for the pyramidal structure having a period of 350 nm, but increased dramatically at wavelengths less than 300 nm. Therefore, we expected that the patterning of sub-wavelength textured structures would eliminate the diffraction-order light, as desired for solar cell applications. Within the working wavelength region of silicon-based solar cells, the pyramidal structure having a period of 350 nm appeared to be suitable for use as an antireflective structure. Figure 2(c) displays the reflectance spectra of pyramidal structures having heights ranging from 200 to 800 nm and a fixed period of 350 nm. Figure 2(d) indicates that the average reflectance of the pyramidal structures decreased rapidly, eventually becoming saturated, upon increasing the height. The average reflectance reduced to less than 1% when the pyramidal structure had a height greater than 500 nm. Figure 2(c) also displays the reflectance spectrum of cylindrical pillars having the same period (350 nm) and a height of 500 nm. The average reflectance of these cylindrical pillars was much higher than that of any of the pyramidal structures. Figure 2(e) displays the average reflectance of cylindrical pillars having a height of 500 nm, a period of 350 nm, and various duty ratios (diameter/period), as simulated using the rigorous coupled-wave method. The cylindrical pillars having a duty ratio of 50% had the minimum reflectance, but the value of about 13% suggests that they are not suitable for use as an antireflective structure for solar cells.
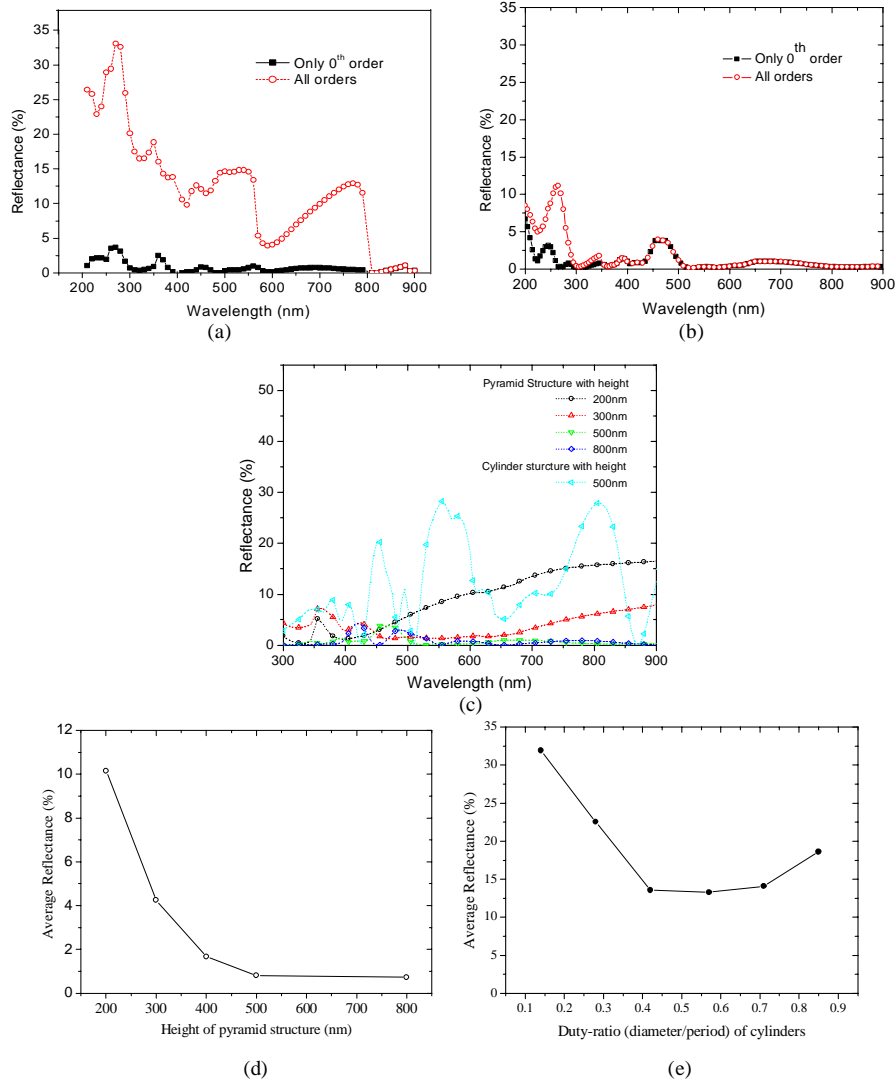
Fig. 2. Simulated reflectance spectra of pyramidal silicon structures: periods of (a) 800 and (b) 350 nm; (c) heights ranging from 200 to 800 nm and a fixed period of 350 nm. (d) Average reflectance of pyramidal structures. (e) Average reflectance of cylinders having various duty ratios, as obtained through rigorous coupled-wave simulation.

To determine the optical behavior of light within the near-field regime propagating on the textured structures, we used the three-dimensional FDTD method to analyze close-packed pyramidal structures of various heights. As indicated in Fig. 3, a plane wave having a wavelength of 366 nm was propagated from 1 μm above the air–silicon interface to the silicon surface in the presence or absence of pyramidal structures. The high absorption of silicon within this range of wavelengths meant that the transmitted light decayed rapidly. Therefore, all of the electric field above z = 1 μm was contributed from the reflective light from the air–silicon interface. Figure 3(a) displays the plane wave that propagated to the air–silicon surface in the absence of pyramidal structures. We find that the apparent reflection electric field existed above the silicon surface. Similarly, Fig. 3(b) displays a plane wave that propagated to the pyramidal structure having a period of 350 nm and a height of 200 nm; we observe that the reflection field had reduced significantly. After increasing the height of the pyramidal

structure to 500 nm, only a small reflection field existed [Fig. 3(c)]. Therefore, the amount of reflected light in the near field was reduced dramatically when utilizing a pyramidal structure having a height of 500 nm; this result is similar to that simulated using rigorous coupled-wave analysis [Fig. 2(c)].
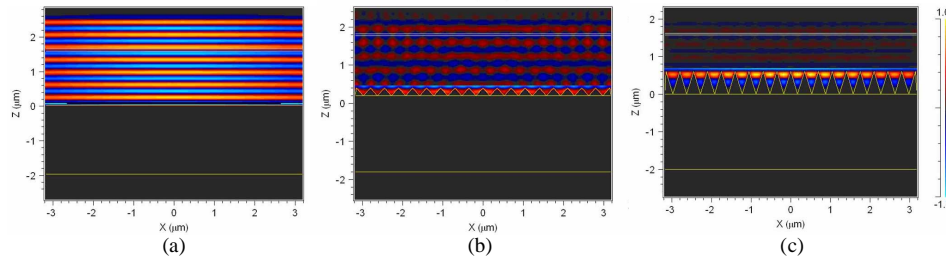
Fig. 3. Plane waves propagated from 1 μm above the air–silicon interface to the silicon surfaces (a) without pyramidal structure and (b, c) possessing (b) 200- and (c) 500-nm-high pyramidal structures.

In the experimental study, we used a dip coater to apply monolayers of polystyrene spheres onto silicon substrates. The patterns of the polystyrene spheres were transferred to the silicon substrates using a reactive ion etcher, the reactive gas O_2 was used to minify the close-packed polystyrene spheres and the reactive gases Cl_2 and SF_6 were used to remove the underlying silicon substrates. Figure 4(a) and (b) present cartoon illustrations of the two- and one-step etching processes, respectively. The two-step etching process—minifying the close-packed polystyrene spheres and then etching the underlying silicon substrate—resulted in cylindrical silicon structures. The one-step etching process involved minifying the close-packed polystyrene spheres and etching the underlying silicon substrate simultaneously. As the size of the polystyrene spheres decreased gradually, the etched area of the underlying silicon increased gradually. Thus, pyramidal silicon structures were readily obtained from the one-step etching process. Because our simulations in Fig. 2(c) suggested that the reflectance of cylindrical pillars was much higher than that of pyramidal structures, in this study we used the one-step etching process to fabricate optimal antireflection structures.
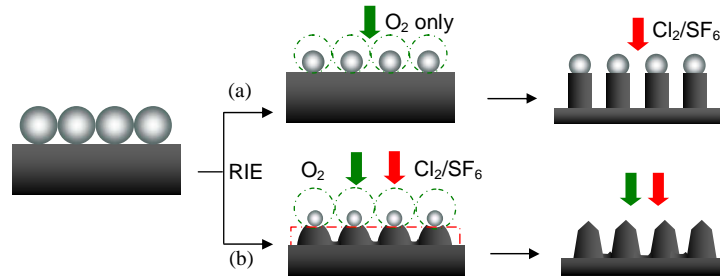
Fig. 4. Schematic illustrations of the (a) two- and (b) one-step etching processes.

Figure 5 (a) displays an image of a close-packed monolayer of 350-nm-diameter polystyrene spheres that were coated on a silicon substrate using a dip coater. Figure 5 (b) and 5(c) present SEM and AFM images, respectively, of the pyramidal structures that were transferred to the silicon substrates after employing the one-step etching process. The period of the pyramidal structure remained as 350 nm and the height was ca. 480 nm. Similarly, we used a monolayer of 200-nm-diameter polystyrene spheres to fabricate pyramidal structures having a period of 200 nm [Fig. 5 (d)]. Figure 6 displays top-view and cross-sectional images of the different textured profiles obtained after varying the duration of etching for the one-step process. Figure 6 (a) indicates that etched silicon having a height of ca. 310 nm and a small, flat roof appeared when the etching was performed for 35 s. Upon increasing the etching

duration, the top of the etched silicon became sharper and the width narrower. Progressing from Fig. 6 (b) to (d), the height of etched silicon increased to 480 nm (60 s) then decreased to 380 nm (150 s). From the top-view images, we observe that the texture area decreased upon increasing the duration of etching.
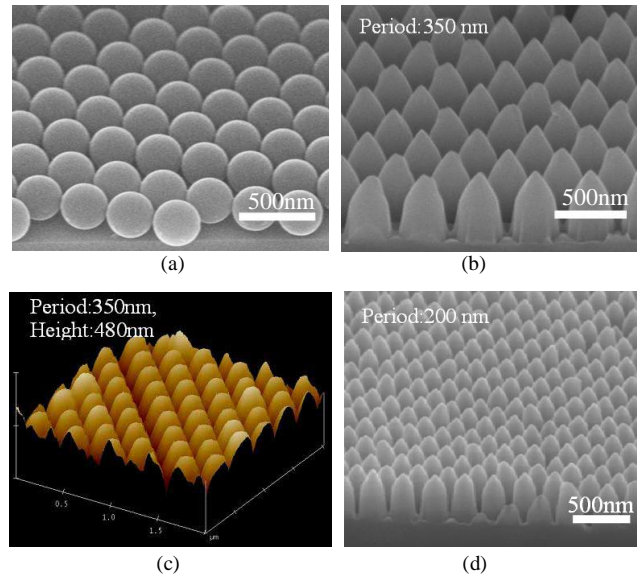
Fig. 5 (a) Close-packed monolayer of 350-nm-diameter polystyrene spheres coated on a silicon substrate. (b) SEM and (c) AFM images of pyramidal structures (period: 350 nm) transferred to silicon. (d) SEM image of pyramidal structures having a period of 200 nm.
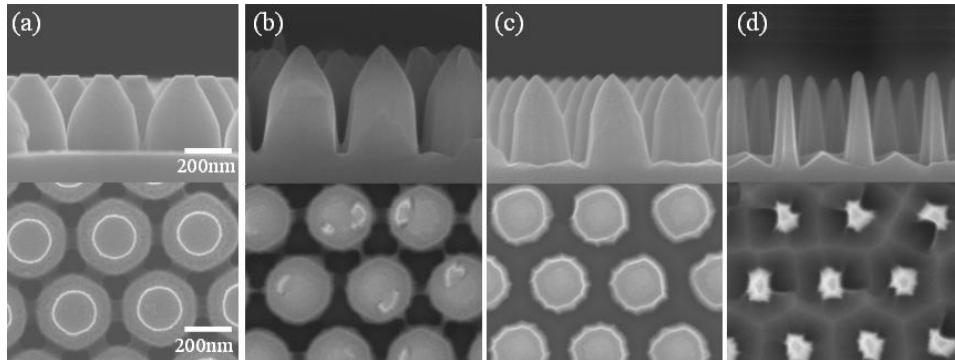
Fig. 6 Top-view and cross-sectional images of the textured profiles obtained after etching for (a) 30, (b) 60, (c) 100, and (d) 150 s using the one-step etching process.

Figure 7 (a) displays the measured reflectance spectra of the textured silicon samples prepared with various durations of etching. The reflectance within the wavelength regime from 350 to 850 nm was less than 2.5% for the sample obtained at an etching duration of 60 s. Figure 7 (b) indicates that the average reflectance and normalized texture area of the etched silicon substrates depended on the duration of etching. The texture areas remained almost constant for etching durations up to 60 s, but decreased rapidly thereafter. The average reflectance decreased upon increasing the etching duration up to 60 s and then increased gradually thereafter. The plot indicates that the optimal minimum average reflectance of less than 1.5% was obtained when the etching duration was 60 s. Similarly, Fig. 7 (c) indicates that the reflectance and height of the etched silicon structures depended upon the duration of etching. The height of the etched silicon structures increased for durations of etching up to 60 s and then decreased gradually thereafter.
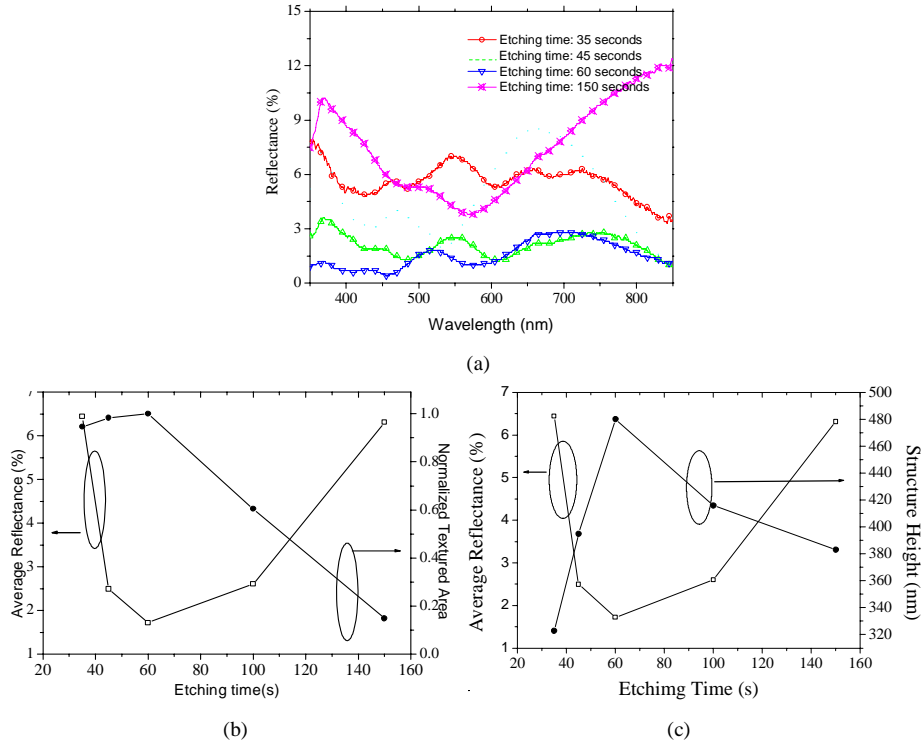
Fig. 7 (a) Measured reflectance spectra of textured silicon samples prepared using various etching durations. (b) Reflectance and normalized texture areas of etched silicon samples plotted with respect to the etching duration. (c) Reflectance and structure heights of etched silicon samples plotted with respect to the etching duration.

Here we propose the possible mechanism for this behavior. The one-step etching process minified the close-packed polystyrene spheres and etched the underlying silicon substrate simultaneously. During the one-step etching process, the size of polystyrene spheres decreased gradually and the height of the etched silicon increased gradually. When the polystyrene spheres had been removed completely, the height of the etched silicon structures would not increase further. In the absence of a covering of polystyrene spheres, the etching rate of the top region of etched silicon would be slightly greater than that at the bottom [23]. Therefore, the heights and widths of the textured structures gradually decreased upon increasing the duration of etching. Furthermore, the textured area of etched silicon would also decrease in the absence of a covering of polystyrene spheres. From our experimental results, we estimate that the duration of etching required to remove the polystyrene spheres completely was ca. 60 s. With their largest height and textured area, the textured structures etched for 60 s exhibited the minimal reflectance.

We have found that utilizing the end-point detection method with the plasma etching process could be used to fabricate textured structures with minimal reflectance. In a plasma etching process, when the material beneath the surface material has begun to be removed, the chemical components in the plasma change as a result of the change in the etch byproducts, signified by a variation in the emission spectrum. Detecting this change using an optical spectrum analyzer allows the end-point to be determined [23]. In this study, we used end-point detection to monitor the total removal of the polystyrene spheres and, thus, to fabricate textured structures having an optimal shape and a large textured area and exhibiting minimal reflectance.

Figs. 8 (a) and 8 (b) display images of the pyramidal structures having heights of 480 and 360 nm, respectively, that we fabricated from polystyrene sphere templates having diameters of 350 and 200 nm, respectively. Figure 8(c) displays the reflection spectra of pyramidal structures having different heights. The reflectance was ca. 10% when the templating single-layer polystyrene spheres had a diameter of 200 nm. Generally, polystyrene spheres having a large diameter can be used to fabricate deeply textured structures that exhibit low surface reflection.
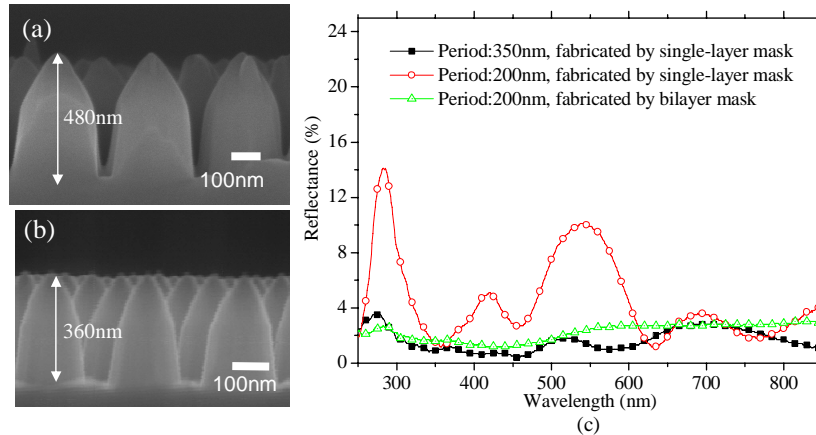
Fig. 8. Pyramidal structures fabricated using templating polystyrene spheres having diameters of (a) 350 and (b) 200 nm. (c) Reflection spectra of pyramidal and honeycomb-like structures.

To increase the etching resistance, we used a bilayer of 200-nm-diameter polystyrene spheres as a template to fabricate structures possessing deeper features. Figure 9 (a) displays an SEM image of the bilayer of polystyrene spheres formed through dip coating of the surface twice. Figure 9 (b) and 9 (c) present schematic top views of the single-layer and bilayer polystyrene spheres, respectively; the darkness of the gray tone represents the effective thickness of the structures—and, hence, the etching resistance during the dry etching process. Thus, bright regions correspond to zones of high etching resistance; therefore, the underlying silicon substrate would be etched initially in the darkest regions. Figures 9 (d) and 9 (e) display SEM images of the textured silicon structures etched for two different durations using the bilayer polystyrene spheres as the template. We observe that honeycomb-like structures formed on the underlying silicon substrate from the dark regions in Fig. 9 (b). Figure 8 (c) indicates that the average reflectance of the honeycombed structure was less than 2%, much smaller than that of the pyramidal structure fabricated from a single layer of 200-nm-diameter polystyrene spheres. These results suggest that bilayer polystyrene spheres can be used as templates for the fabrication of sub-wavelength honeycomb-like structures exhibiting low reflectance.

(a)

(b)

(c)

(d)

(e)
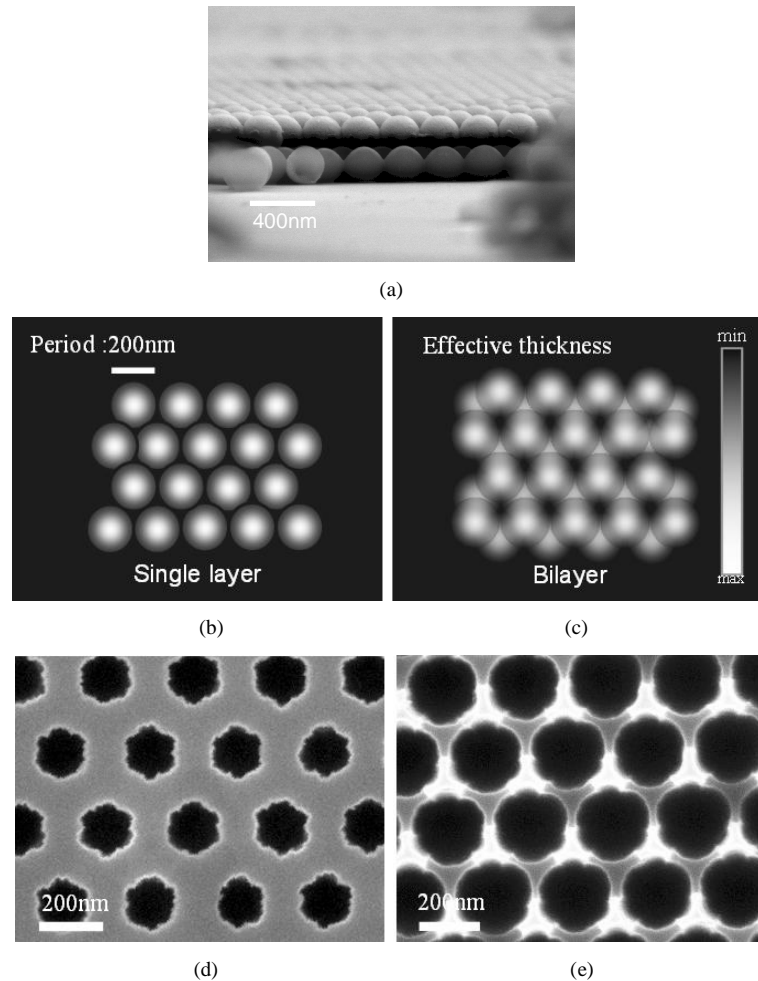
Fig. 9. (a) SEM image of a bilayer of polystyrene spheres. Schematic representations of (b) single-layer and (c) bilayer assemblies of polystyrene spheres. SEM images of textured silicon structures etched using a bilayer of polystyrene spheres as the template and etching durations of (d) 50 and (e) 100 s.

4. Conclusion

The key issue when attempting to increase the external quantum efficiency of semiconductor-based solar cells is reducing interfacial reflection in the solar cell working-wavelength regime. The efficiency of solar cells can be improved by using texturing pyramidal and honeycomb-like structures exhibiting minimal reflection. Using rigorous coupled-wave analysis, we found that the reflection of the textured structures increased dramatically with respect to the diffraction order. In addition, the reflectance decreased upon increasing the height of the pyramidal features. From simulations, we predicted that the reflectance would be reduced to less than 1% when the pyramidal features had a height of 500 nm; in contrast, cylindrical pillars having the same period and height would not reduce the reflectance to less than 10%. From an analysis of the pyramidal structures using the three-dimensional FDTD method, we found that the reflection of light in the near field could also be reduced dramatically by a pyramidal structure having a height of 500 nm; this finding is similar to the result simulated by the rigorous coupled-wave analysis. In experimental studies, we used polystyrene spheres of sub-wavelength scale to pattern sub-wavelength textured structures to eliminate diffraction-order light. We utilized a simple method, combining close-packed monolayer and bilayer

polystyrene spheres with a one-step reactive ion etching process, to fabricate optimized pyramidal and honeycomb-like antireflection structures, respectively. Using the end-point detection method during the plasma etching process allowed us to monitor the fabrication process to select textured structures exhibiting minimum reflectance. Sub-wavelength pyramidal and honeycomb-like structures exhibiting reflectance less than 1.5% were readily obtained without the need for any lithography equipment.